Design of Misalignment Tolerant Control for an Inductive Charger with V2G Possibilities

Vermeer, W.W.M.; Bandyopadhyay, S.; Bauer, P.

DOI
10.1109/WoW45936.2019.9030618

Publication date
2020

Document Version
Final published version

Published in
2019 IEEE PELS Workshop on Emerging Technologies

Design of Misalignment Tolerant Control for an Inductive Charger with V2G Possibilities

Wiljan Vermeer*, Soumya Bandyopadhyay*, Pavol Bauer*
*DC Systems, Energy Conversion & Storage, dept. Electrical Sustainable Energy
Delft University of Technology
Delft, the Netherlands
w.w.m.vermeer@tudelft.nl, s.bandyopadhyay-1@tudelft.nl, p.bauer@tudelft.nl

***Abstract*—Since the power transfer efficiency in inductive power transfer (IPT) systems is directly related to the coupling of the transformer, coil misalignment can drastically decrease the efficiency. In this paper a misalignment tolerant control scheme is proposed which tracks the maximum power transfer efficiency point under misalignment. It does this by matching the impedance of the load with respect to the transformer based on an online coupling factor estimation, as well as tracking the resonance of the system. The control scheme is implemented on a series-series compensated system and designed such that it can be operated bidirectionally in the future, however this is not in the scope of this paper. The proposed control results in an overall efficiency improvement of 5% and 23% under 0 and 8 cm misalignment, respectively, compared to a constant rectifier output voltage of 48V.**

***Index Terms*—inductive power transfer, misalignment, tolerant, bidirectional, V2G.**

I. Introduction

In the future, wireless charging of electric vehicles (EVs) is expected to have a role in the energy transition. As it offers the possibility for opportunity charging at traffic signs and taxi/bus stops and can therefore be used as range extender. Which reduces the range anxiety of potential EV drivers, which is a major hold back for mass EV adaptation [1]. Another development is the emergence of bidirectional chargers, in order to enable the so called vehicle-to-grid (V2G) operation. During V2G operation the EV is integrated into the power grid and can be used as a power source for ancillary services, used for balancing the intermittent nature of renewable energy sources in the grid [2]. By extending an inductive charger with V2G possibilities, the availability of both inductive charging and ancillary services is improved. However, in every inductive power transfer system the power transfer efficiency is directly related to the coupling between the coils [3]. In the case of an EV charger this is variable as the EV will not always be fully aligned with the transmitter coil.

Therefore, this paper proposes a control method which tracks the maximum power transfer efficiency point during coil misalignment. The proposed control method consists of three parts: 1. Resonance tracking, 2. Impedance matching and 3. Output power control. Previous studies assume a fixed resonant frequency when talking about a maximum power transfer efficiency [4] [5] [6]. However, even though series-series compensation is used, it was found that misalignment can change the self-inductance of the transformer (for a DD-coil structure). Hereby changing the resonant frequency, decreasing the power transfer capability and efficiency [7] [8]. Therefore, the main contribution of this paper is the derivation of a misalignment tolerant control which includes resonant tracking but also coupling factor estimation and controller design for a bidirectional converter. Furthermore, it will be shown that using this control method, bifurcation will always be avoided in the entire possible operating range. The system will be designed for bidirectional power flow such that V2G operation is possible. In the first section some background knowledge about impedance matching and bifurcation will be presented, next the proposed control is discussed, followed by the controller design and finally the experimental results are discussed.

II. Background

A. Impedance Matching

In a Thevenin equivalent circuit, maximum power is transferred to the load when the Thevenin resistance R_{th} equals the load resistance R_L. The same holds for an inductive power transfer system, such as the equivalent circuit shown in Figure 1. Here the Thevenin source is the induced voltage in the secondary coil and the Thevenin resistance is comprised of all the losses in the secondary side (core, winding, capacitor and shielding). In Figure 1 R_L is the AC equivalent load resistance seen by the secondary side consisting of the rectifier and its load. The voltage equations of this equivalent circuit under resonance are shown in eq. (1).

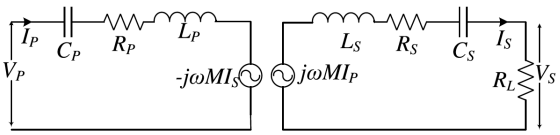

Fig. 1: Equivalent circuit of a series-series compensated resonant tank with AC equivalent load resistor R_L

$$\begin{bmatrix} V_p \\ V_s \end{bmatrix} = \begin{bmatrix} R_p & -j\omega_0 M \\ j\omega_0 M & -(R_s + R_L) \end{bmatrix} \begin{bmatrix} I_p \\ I_s \end{bmatrix} \tag{1}$$

Here $V_{p/s}$ are the primary and secondary side voltage, M is the mutual inductance and $R_{p/s}$ are the primary and secondary losses. These losses were determined using a FEM model of

978-1-5386-7514-4/19/$31.00 ©2019 IEEE

the transformer [9] and experiments. These losses are current dependent, however this change is negligible. As with the Thevenin equivalent circuit, maximum power is transferred to the load when the AC equivalent load equals the losses inside the secondary side of the resonant tank. Under resonance this equals:

$$R_{L,\eta_{max}} = \omega_0 M + R_s \tag{2}$$

B. Bifurcation

When bifurcation occurs the system becomes a fourth order system with two resonant frequencies this is shown in Figure 2). This happens for certain ratio's of resonant tank quality factors Q_p and Q_s, as defined in eq. (11) and (12) [8]. Bifurcation reduces the voltage gain and hereby the power transfer capability of the system. Furthermore it also adds complexity to the control of the system, therefore it is often desired to avoid bifurcation.

$$Q_P = \frac{L_p(R_{L,eq} + R_S)}{\omega_0 M^2} \tag{3}$$

$$Q_S = \frac{\omega_0 L_s}{R_{L,eq} + R_S} \tag{4}$$

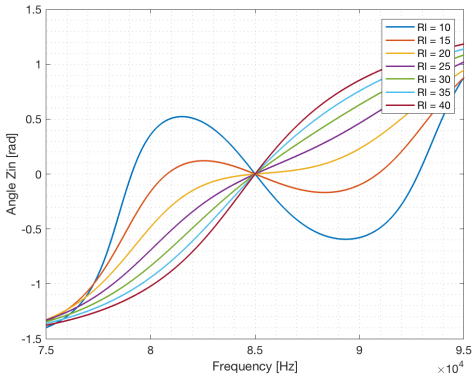

Fig. 2: Input impedance angle over frequency for a varying load resistance; introduction of multiple zero phase angle frequencies when bifurcation occurs.

In a misalignment tolerant system where the mutual inductance M is variable and the proposed control scheme is varying $R_{L,eq}$ accordingly, the bifurcation limit might be exceeded. Therefore, it is important to determine the limits at which bifurcation occurs to assess the effect of the proposed control scheme on bifurcation. In [8] and [7] the limits at which bifurcation occurs were determined. These limits are shown in eq.(13).

$$Q_p \leq \frac{4Q_s^3}{4Q_s^2 - 1} \quad \& \quad Q_p > \frac{1}{Q_s} \tag{5}$$

III. System Architecture & Proposed Control

Figure 3 shows the total system and its control scheme, the parameters are shown in Table I. The resonant tank was designed to be symmetrical such that the control is similar for both directions of power. The control scheme is also symmetrical, however the resonance tracker is only operating at the side which acts as inverter. Furthermore, during charging the secondary (EV) side dc/dc converter acts as impedance matching controller and calculates the setpoint as shown in the Fig. 3, while the primary side dc/dc controller receives the voltage setpoint from the secondary side. During V2G operation the operation is the opposite (the EV side is used as inverter and power control, and the grid side is used for impedance matching controller and determines the voltage setpoint). The goal of the control scheme is to track the maximum power transfer efficiency point of the inductive link. For any wireless link based on resonant inductive coupling, there are two requirements for maximum power transfer efficiency 1. Operating the inverter at the resonance frequency, the input impedance Z_{in} seen by the inverter is at its minimum since it is purely resistive therefore no circulating currents occur. Furthermore, inverter and rectifier switching losses are minimized due to almost zero voltage/current switching. Secondly, 2. The impedance of the secondary side resonant tank should be matched to the load [5]. Therefore the total control scheme is divided into three parts: 1. Impedance matching, 2. Resonant tracking and 3. Output power control.

TABLE I: Setup parameters

Symbol	Quantity	Value
V_{in}	Input Voltage	350V
V_{bat}	Battery Voltage	48V
L_P	Primary Inductance	200 μH
L_S	Secondary Inductance	200 μH
C_P	Primary Capacitance	18.9 nF
C_S	Secondary Capacitance	18.9 nF
$V_{1,dc}$	Grid side DC link voltage	50-120V
$V_{1,dc}$	Battery side DC link Voltage	50-120V
$f_{sw,inv}$	Inverter switching frequency	80-90 kHz
$f_{sw,dc}$	Dc/dc converter switching frequency	50 kHz
P_{out}	Output power	500W
l_{gap}	Airgap length	11 cm

A. Impedance Matching

Then from [5] it is known that the equivalent load resistance equals eq. (3). This shows that the maximum power transfer efficiency can be controlled by the rectifier output voltage $U_{2,dc}$.

$$R_{L,eq} = \frac{8}{\pi^2 \eta_{rect}} R_L = \frac{8}{\pi^2} \frac{V_{2,dc}^2}{P_2} \tag{6}$$

Then by substituting eq. (3) into eq. (2) the resulting voltage setpoint can be determined as shown in eq. (4).

$$U_{2,dc} = \sqrt{\frac{\pi^2 \eta_{rect}}{8} \left(\omega_0 M + R_s\right) P_2^*} \tag{7}$$

Here $V_{2,dc}$ is the rectifier output voltage, η_{rect} is the rectifier efficiency, P_2 is the rectifier output power setpoint and $\omega_0 M + R_s$ is the magnitude of the total impedance of the secondary side in resonance. Using the secondary side dc/dc converter $V_{2,dc}$ can be controlled to this setpoint. From eq.(4) it is clear that in order to calculate the voltage setpoint, the power setpoint and the mutual inductance needs to be known. The power setpoint is given to the controller, however the

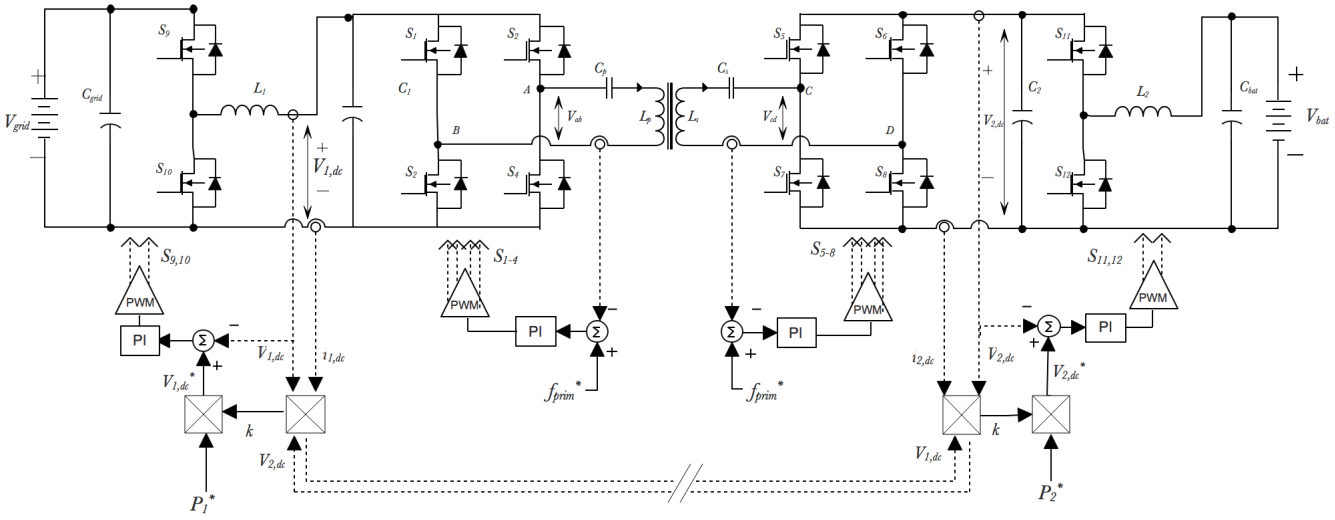

Fig. 3: Total control scheme: 2 frequency controllers and 2 voltage controllers; for impedance matching and output power control.

coupling factor should be estimated, this is discussed in the next subsection.

1) Coupling Factor Estimation: Using the voltage equations of the inductive link in resonance (eq.(1)), while substituting $M = k\sqrt{L_p L_s}$ the following relation for k can be determined [10].

$$k = \frac{V_p + \sqrt{V_p^2 - 4R_p I_s\left(V_s + R_s I_s\right)}}{2I_s\omega_0\sqrt{L_p L_s}} \tag{8}$$

By substituting the DC Fourier equivalent values of the primary and secondary currents and voltages, as shown in eq. (6) and (7), the coupling factor can be estimated using the primary and secondary DC link voltages and currents as shown in eq. (8)

$$V_{prim} = \frac{2\sqrt{2}}{\pi}V_{1,dc} \tag{9}$$

$$V_{sec} = \frac{2\sqrt{2}}{\pi}V_{2,dc} \tag{10}$$

$$k = \frac{4V_{1,dc} + \sqrt{16V_{1,dc}^2 - \pi R_p i_{2,dc}\left(8V_{2,dc} + \pi^2 R_s i_{2,dc}\right)}}{\pi^2 i_{dc,2}\omega_0\sqrt{L_p L_s}} \tag{11}$$

Here $V_{1,2,dc}$ and $I_{1,2,dc}$ are the primary and secondary DC link voltages and currents and $L_{p,s}$ $R_{p,s}$ are the inductance's and losses of the resonant tank. Finally ω_0 is the switching frequency which in the coupling estimation is assumed to be constant at the resonance frequency of 85kHz. However this frequency actually varies when the coils are misalignment. Therefore, in order for all of the above equations to be valid and in order to achieve maximum power transfer the resonance frequency is tracked.

B. Resonance Tracking

Even though series-series compensation is used, which is independent of the alignment of the coils, the resonant frequency still varies when the coupling between the coils changes. This is because the spatial orientation and vicinity of the secondary coil, affects the self inductance of the primary coil, and vice versa. The resonance frequency is tracked by measuring the phase between the gate voltage and the zero crossing of the primary current [11]. The circuit used for this is shown in Figure 4.

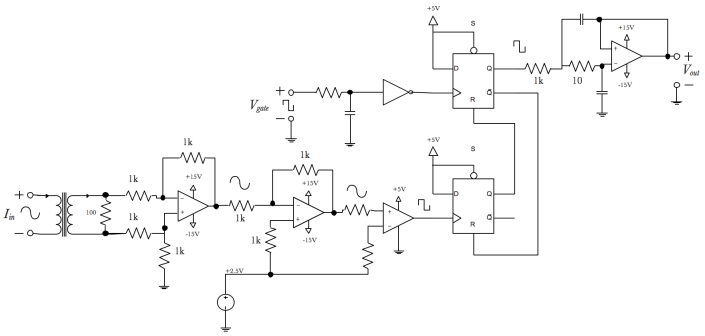

Fig. 4: Circuit used to measure the phase between V_{gate} and I_{prim} [11], the DC output voltage V_{out} is send to a PI controller which controls it to a reference for ZVS.

The current is measured using a current transformer and a shunt resistor. This voltage is then lifted with 2.5V (in order for the comparator input to be positive) after which it is compared to the same 2.5V reference. The resulting voltage is a square wave which is positive when the primary current is positive. This square wave voltage is compared to the inverted gate voltage using two d type flip-flops. In order to obtain a linear phase-voltage relationship [11] the gate voltage is inverted, such that a lagging current has a measured phase between $[0, \pi]$ and a leading current has a measured phase between $[\pi, pi]$. The resulting output of the flip-flop is a square wave

of which its duty cycle is equal to the phase difference between V_{gate} and I_{prim}. This is then filtered to obtain a DC output which is related to the phase. This voltage is send to the microcontroller of the inverter, here the mean value of the input is taken in order to counteract for jitter and noise. Finally, the switching frequency is controlled by controlling v_{phase} to a reference voltage corresponding to ZVS.

C. Power Control

The final part of the proposed control scheme is the control of the output power. This is done by controlling the inverter input voltage. The advantage of this method over e.g. frequency control or phase shift modulation, is that the system can stay in resonance over the whole power range. Furthermore, ZVS is possible for both turn-on and -off over the whole power range. The voltage setpoint for the primary DC link is based on the maximum transfer efficiency requirement for the primary coil self-inductance, as stated in [5]

$$L_1 = L_2\left(\frac{U_{1,dc}}{U_{2,dc}}\right)^2 \Rightarrow U^*_{1,dc} = \frac{1}{\eta}U_{2,dc} \tag{12}$$

Where $\frac{1}{\eta}$ is the efficiency of the inductive link, which can be determined using a look-up table based on the power/voltage setpoint. This way no feedback is needed from the secondary side.

D. Effect of Impedance Matching on Bifurcation

In order to asses the effect of the control on bifurcation the first condition of eq. (5) is rewritten in terms of R_L and k by substituting eq. (3) and (4). The result is shown in Figure 5 and it shows that using the impedance matching control, bifurcation will always be prevented for this system. Note that since $L_p = L_s$ the second condition in eq. (5) is always valid.

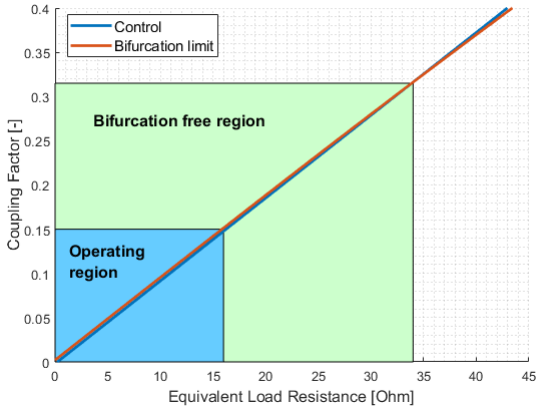

Fig. 5: Bifurcation free region and operating region. Bifurcation is avoided within the possible operating region

IV. Controller Design

Next the controllers are designed. In total there are 4 controllers: 2 voltage controllers and 2 frequency controllers. The maximum gain of the frequency controllers is dependent on the amount of jitter in the resulting frequency, therefore these controllers are tuned experimentally. Since the control of $V_{1,dc}$ is interfering with $V_{2,dc}$ an analytical model for the two voltage controllers is determined. Because of this interference the control of $V_{2,dc}$ should be an order of magnitude faster than $V_{1,dc}$ for the perturbance caused by $V_{1,dc}$ to be negligible. To do this the $\frac{V_{2,dc}}{d_1}$ and $\frac{V_{2,dc}}{d_2}$ frequency response is determined (Here $d_{1,2}$ are the duty cycles of both dc/dc converters). The $\frac{V_{2,dc}}{d_1}$ response is determined by combining the small signal model of dc/dc1 and the inductive link. The model of the inductive link is based on the extended describing function method, as derived in [12]. This is combined with the small signal model of the dc/dc converters operating in buck mode by rewriting the C and D state space matrices using only state variables and equating the in- and output of the models. The resulting $\frac{V_{2,dc}}{d_1}$ and $\frac{V_{2,dc}}{d_2}$ bode plots are shown in Figure 6 and 7. For the secondary dc/dc converter a bandwidth of $\omega_{c,1} = 2600$ rad/s is selected. Therefore, in order to avoid interference the bandwidth of the primary controller has to be $w_{c,2} \leq \frac{1}{10w_{c,1}} = 200$ rad/s. Figures 6 and 7 show that both plant responses have a $0dB/dec$ slope around the crossover frequency, therefore a type 1 PI controller can be used for both controllers [13] which has the following transfer function:

$$C(s) = K\frac{1+\tau s}{\tau s} \tag{13}$$

The secondary controller is designed such that the loop transfer function (LTF) has 0dB gain at the cross-over frequency [14], i.e.:

$$20log(G_c(w_{c,2})) + 20log(G_p(w_{c,2})) = 0 \tag{14}$$

Which results in $K_2 = 4.47 \times 10^{-3}$. Furthermore, for the LTF of the secondary controller a phase margin (PM) of 60° is selected for adequate damping [14].

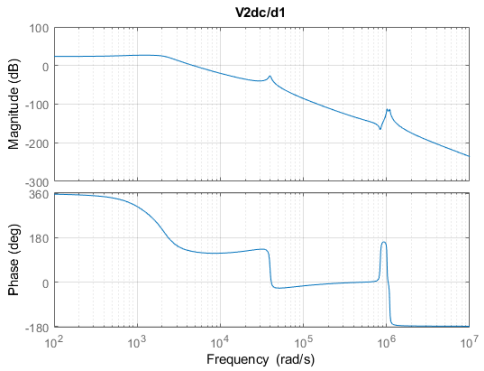

Fig. 6: Open loop frequency response of $\frac{V_{2,dc}}{d_2}$

The time constant τ in eq. (13) can than be calculated according to eq. (15)-(16).

$$\phi = PM_{LTF} - (180 + \angle G_s(w_c)) \tag{15}$$

$$\tau = \frac{tan(\phi + 90°)}{w_c} = 3.06 \times 10^{-4} \tag{16}$$

This results in the LTF bode plot shown in Figure 8. Note that the phase margin is displayed as $PM_2 = -121°$, however

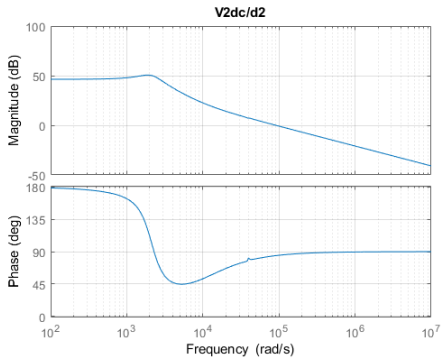

Fig. 7: open loop frequency response of $\frac{V_{2,dc}}{d_1}$

this corresponds to a PM of $60°$ since the plant's phase is shifted with $180°$ because the controller is controlling its input voltage. Next, the primary controller is tuned such that only a single crossover frequency exists which is below 260 rad/s. Using $K_1 = 0.02$ and $\tau = 0.0015$ a LTF PM of $102°$ at 219rad/s was achieved.

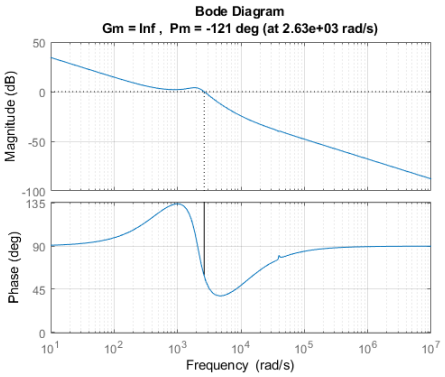

Fig. 8: Loop Transfer Function of $\frac{V_{2,dc}}{d_2}$

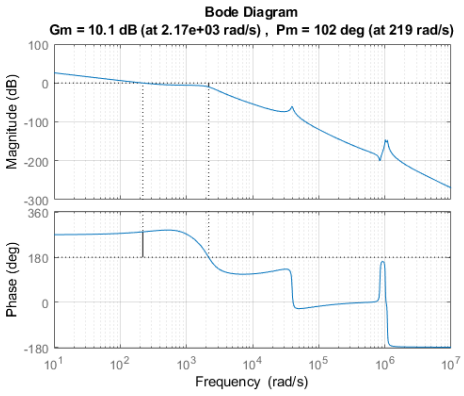

Fig. 9: Loop Transfer function $\frac{V_{2,dc}}{d_1}$

In order to test the controller the setup was implemented in MATLAB Simscape. In Figure 10 a step response in $V_{1,dc}$ is shown with a open loop and closed loop secondary side, respectively. The large initial peak is due to the inrush current and the relatively slow response of the primary controller. From Figure 10 it is clear that even for a large perturbation in $V_{1,dc}$ the secondary controller can maintain a constant voltage.

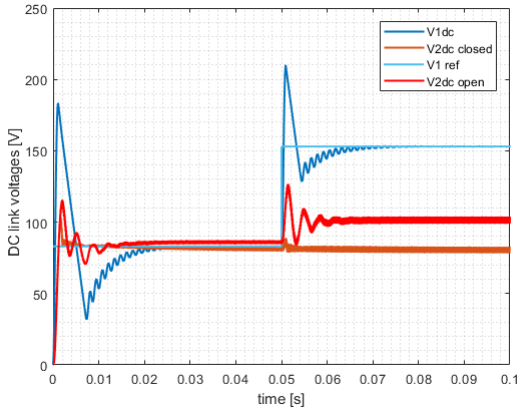

Fig. 10: Closed and open loop response of $V_{2,dc}$ on a step change in $V_{1,dc}$. The controller is keep $V_{2,dc}$ constant.

V. Results

Finally, the control was tested on a laboratory setup. A picture of this setup is shown in Figure 12.

A. Impedance Matching

In Figure 11 the overall system efficiency is shown for multiple misalignment, with and without the control. When no control is used the output of the rectifier is connected directly to the 48V electronic load. The efficiency with control includes the losses of the additional dc/dc converter. Under no misalignment the efficiency improvement is about 5%, while under 8cm misalignment the efficiency improvement is approximately 23%. This verifies the operation of the proposed control system. These measurements were performed at 300W, in a system which mostly has been designed for several kW's. The overall resulting efficiency is therefore low. However, the efficiency improvement will only increase for higher output power, since this would have required a higher secondary DC link voltage according to eq.(4).

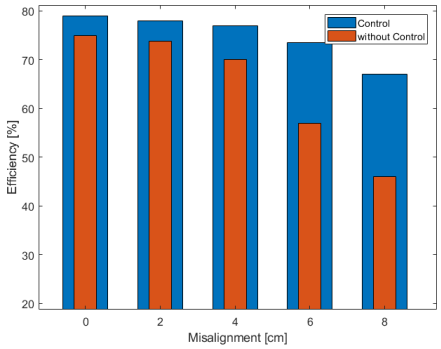

Fig. 11: Overall efficiency with- and without control up to 8 cm misalignment. The control improves the efficiency by 5% for perfect alignment, and 23% under 8 cm misalignment.

B. Coupling estimation

Figure 13 shows the result of the online coupling estimation. In order to minimize contamination due to noise and jitter, the mean value of the measurements is taken inside the

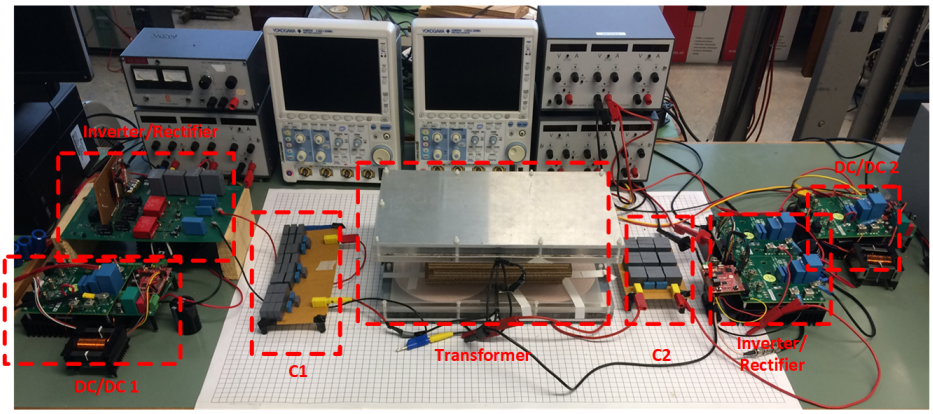

Fig. 12: Experimental setup

microcontroller. However some noise was still noticeable, for further reduction Kalman filtering has to be used [6].

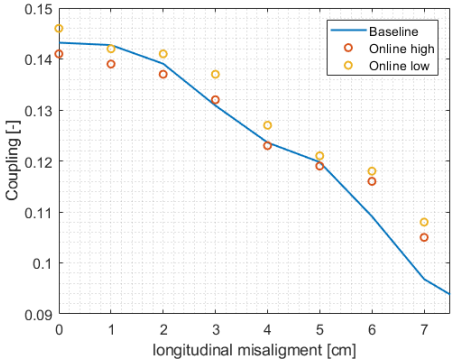

Fig. 13: High and low limit of the online coupling estimation compared to a baseline measurement.

C. Resonance tracking

In Figure 14 the phase measurement for a lagging current is shown. Here the sinusoidal current is the actual current measured using a 100MHz probe. From this figure it can be seen that the latency between the actual current and the comparator output is negligible this shows that there is negligible latency in the circuit and that the phase is measured accurately.

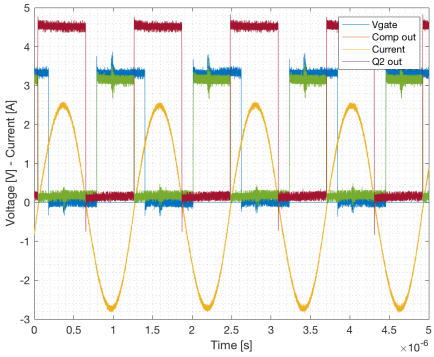

Fig. 14: Phase Measurement of a lagging current. Flip flops are triggered by rising gate voltage (blue) and reset by a positive current (yellow).

VI. Conclusion

In this paper a control method was proposed which tracks the maximum power transfer efficiency of an inductive charger for electric vehicles. This was done by tracking the resonance frequency and matching the equivalent AC load seen by the resonant tank to the secondary side resonant tank impedance. The experimental results show that an efficiency improvement of $5-23\%$ is possible. In order to do this the coupling factor between the transformer coils was estimated based on the DC link voltages and current, this gave an accurate result up to 6 cm misalignment. Furthermore a successful phase measurement circuit was designed which was used to track the resonance current and adapt the inverter switching frequency accordingly.

References

[1] Z. Bi, T. Kan, C. C. Mi, Y. Zhang, Z. Zhao, and G. A. Keoleian, "A review of wireless power transfer for electric vehicles: Prospects to enhance sustainable mobility," *Applied Energy*, vol. 179, pp. 413 – 425, 2016.

[2] K. H. T. Markel, A. Meintz, "Multi-Lab EV Smart Grid Integration Requirements Study," pp. 1–8, May 2015.

[3]

[4] W. Zhang, S. Wong, C. K. Tse, and Q. Chen, "Analysis and comparison of secondary series- and parallel-compensated inductive power transfer systems operating for optimal efficiency and load-independent voltage-transfer ratio," *IEEE Transactions on Power Electronics*, vol. 29, no. 6, pp. 2979–2990, June 2014.

[5] R. Bosshard, J. W. Kolar, and B. Wunsch, "Control method for inductive power transfer with high partial-load efficiency and resonance tracking," pp. 2167–2174, May 2014.

[6] T. I. D. Kobayashi and Y. Hori, "Real-time coupling coefficient estimation and maximum efficiency control on dynamic wireless power transfer for electric vehicles," pp. 1–6, 2015.

[7] M. Kok, R. Fajtl, and J. Lettl, "Analysis of bifurcation in two-coil inductive power transfer," pp. 1–8, July 2017.

[8] C. Wang, G. A. Covic, and O. H. Stielau, "Power transfer capability and bifurcation phenomena of loosely coupled inductive power transfer systems," *IEEE Transactions on Industrial Electronics*, vol. 51, no. 1, pp. 148–157, 2004.

[9] S. Bandyopadhyay, V. Prasanth, L. R. Elizondo, and P. Bauer, "Design considerations for a misalignment tolerant wireless inductive power system for electric vehicle (ev) charging," pp. P.1–P.10, 2017.

[10] V. Jiwariyavej, T. Imura, and Y. Hori, "Coupling coefficients estimation of wireless power transfer system via magnetic resonance coupling using information from either side of the system," *IEEE Journal of Emerging and Selected Topics in Power Electronics*, vol. 3, no. 1, pp. 191–200, March 2015.

[11] Y. Jang, Y. Wang, J. Liu, X. Li, and L. Wang, "An accurate phase detection method for realizing zvs of high frequency inverter in wireless power transmission," pp. 1380–1384, June 2017.

[12] Z. U. Zahid, Z. Dalala, and J. J. Lai, "Small-signal modeling of series-series compensated induction power transfer system," pp. 2847–2853, March 2014.

[13] K. Aditya, "Design and implementation of an inductive power transfer system for wireless charging of future electric transportation," August 2015.

[14] K. Aditya and S. S. Williamson, "Advanced controller design for a series-series compensated inductive power transfer charging infrastructure using asymmetrical clamped mode control," pp. 2718–2724, 2015.